Centered Honeycomb NiSe2 Nanoribbons: Structure and Electronic Properties

ARTICLE *in* THE JOURNAL OF PHYSICAL CHEMISTRY C · FEBRUARY 2014

Impact Factor: 4.77 · DOI: 10.1021/jp409504f · Source: arXiv

3 AUTHORS:

Jose Angel Reyes-Retana
Universidad Iberoamericana Ciudad de México
9 PUBLICATIONS **27** CITATIONS
SEE PROFILE

Gerardo G. Naumis
Universidad Nacional Autónoma de México
130 PUBLICATIONS **956** CITATIONS
SEE PROFILE

Felipe Cervantes-Sodi
Universidad Iberoamericana Ciudad de México
18 PUBLICATIONS **955** CITATIONS
SEE PROFILE

THE JOURNAL OF PHYSICAL CHEMISTRY C

Article

pubs.acs.org/JPCC

Centered Honeycomb $NiSe_2$ Nanoribbons: Structure and Electronic Properties

J. A. Reyes-Retana,*[,†] G. G. Naumis,[†] and Felipe Cervantes-Sodi[‡]

[†]Departamento de Física-Química, Instituto de Física, Universidad Nacional Autónoma de México (UNAM), Apartado Postal 20-364, 01000 México, Distrito Federal, México

[‡]Departamento de Física y Matemáticas, Universidad Iberoamericana, Prolongación Paseo de la Reforma 880, Lomas de Santa Fe, 01219, DF, México

Supporting Information

ABSTRACT: Quasi-one-dimensional nanoribbons are excellent candidates for nanoelectronics and as electrocatalysts in hydrogen evolution reactions; therefore, we investigate by means of density functional theory the structure and electronic properties of a new kind of one-dimensional ribbons, namely, centered honeycomb $NiSe_2$ nanoribbons. Depending on the crystallography and atomic composition of the edges, it is shown that these ribbons can belong to one of six zigzag or two armchair families. In the zigzag families, after edge reconstruction, all the bare ribbons are metallic. Hydrogen passivation produces band gaps in two of the six families by sweeping edge states, corresponding to the stablest nanoribbons. For the armchair nanoribbons, the geometrical reconstruction leads to semiconductors with small band gap, and the hydrogen passivation of the edges increases the band gap up to ~0.6 eV. The inclusion of the spin−orbit interaction tends to reduce the band gaps, and the systems become metallic in the bulk limit. Several mechanisms are seen to determine band structure and stability: quantum confinement, edge states, density of broken bonds, and asymmetry with respect to the central line. As a result, some terminations are stable; others present edge reconstruction while SeH_2 molecules are prone to desorb from the ribbon's edges.

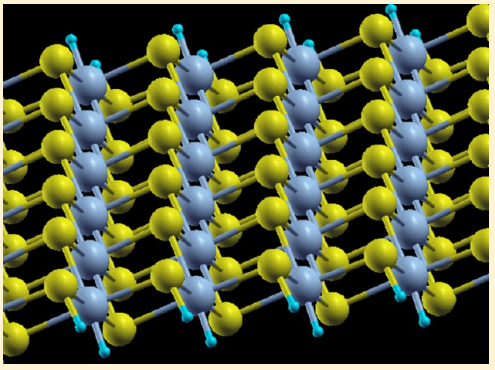

INTRODUCTION

Two-dimensional transition-metal dichalcogenides (2D-MX_2) materials are a variation of transition-metal dichalcogenides[1,2] which are three-dimensional (3D) versatile layered compounds with a wide range of electrical and optical properties of the narrow *d* band type. As graphite, composed of graphene layers, transition-metal dichalcogenides are composed of sandwich-type layers consisting of a sheet of hexagonal close-packed transition-metal atoms between two sheets of hexagonal close-packed chalcogen atoms.[3]

Bulk materials present different properties when isolated as atom thick 2D crystals.[4,5] For example, layered centered honeycomb compounds present catalytic behavior[6,7] higher than their bulk form and graphene, the undisputed landmark example,[5,8] exhibits enhanced thermal and electrical conductivity compared with those of graphite. Recent developments in 2D materials have allowed their synthesis by mechanical exfoliation,[9,5] chemical vapor deposition (CVD),[10,11] or liquid exfoliation.[12,13] Furthermore, it has been shown that feasible electronics involving graphene will include the integration of materials,[14] such as silicene, germanene,[15] BN honeycomb sheets,[5,16] III−V binary compounds, metallic oxides, and 2D transition-metal dichalcogenides (2D-MX_2). The main reason to use other 2D materials different from graphene is that altough a pseudogap can be opened in graphene by chemical doping,[17−20] applying electromagnetic fields,[21,22] or cutting it into nanoribbons, graphene does not have an intrinsic electronic bandgap.

MoS_2 and $MoSe_2$ single layers have been successfully isolated, attracting much attention because of their direct band gaps of 1.90[23] and 1.55 eV,[24] respectively. Recent studies show that these systems could be promising for novel optoelectronics devices, such as two-dimensional light detectors and emitters.[25] Furthermore, Lukowski et al.[6] and Voiry et al.[7] have recently shown that both MoS_2 and WS_2 exfoliated nanosheets in the strained metallic centered honeycomb T structure are highly effective as electrocatalists in the hydrogen evolution reaction. This effect is due to the high density of active sites at the edges of the nanosheets in the T structure, representing the first application of the metallic T polymorph of layered metal chalcogenides in catalysts.[6,7] As for graphene and other 2D materials[8] that can be cut as quasi-one-dimensional (1D) structures in the form of nanoribbons,[26−28] some 2D-MX_2 and metal oxides also exist as 1D structures or nanoribbons.[29] Because of quantum confinement effects, particularly at the edges,[27,28] 1D compounds present properties

Received: September 23, 2013
Revised: January 15, 2014

   dx.doi.org/10.1021/jp409504f | J. Phys. Chem. C XXXX, XXX, XXX−XXX

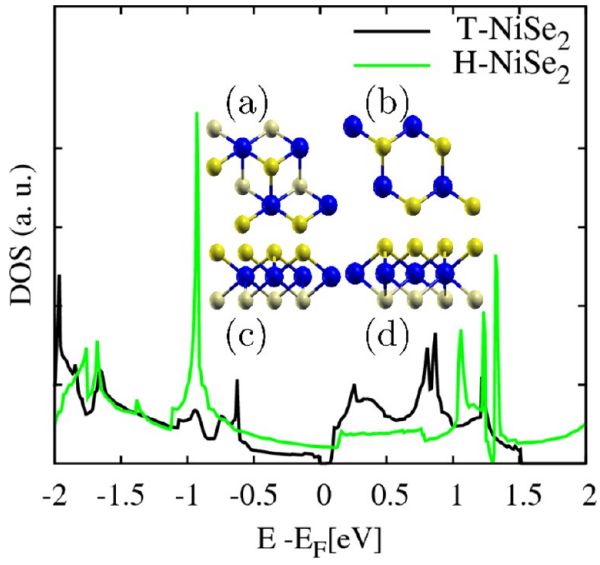

Figure 1. Electronic density of states without spin−orbit interactions and structure for the honeycomb (H) and centered honeycomb (T) lattices. Insets (a) and (b) are the T and H structures in the *xy* plane, respectively. Insets (c) and (d) display the T and H structures in the *xz* plane, respectively. We use slightly different colors to indicate which Se atoms are in the bottom layer (light yellow) and which are in the top layer (yellow). Ni atoms are in the middle layer (blue).

different than those of bulk MX_2 and 2D-MX_2; thus, it is important to study the electronic properties of nanoribbons.[6] Some properties of 1D-MX_2 have been recently studied. For example, MoS_2 nanoribbons and their defects have been explored to give different functionalizations depending on the edge, pressure, and electric field.[30−32] Other metallic chalcogenide nanoribbons have been experimental obtained, such as Bi_2Se_3[33] and CuTe.[34]

Density functional theory (DFT) studies reveal that several of these 2D-MX_2 compounds are stable or metastable in one of two possible crystallographic structures; honeycomb (H) and centered honeycomb (T).[3,35−37] A diagram of such structures appears in Figure 1. Up to now, most of the studies on 2D-MX_2 and their ribbons are on H-structure compounds. However, according to Ataca et al.,[3] SeO_2, SeS_2, $ScSe_2$, $ScTe_2$, TiS_2, $TiSe_2$, $TiTe_2$, VS_2, VSe_2, VTe_2, MnO_2, MnS_2, $MnSe_2$, $MnTe_2$, NiO_2, NiS_2, $NiSe_2$, $NiTe_2$, NbS_2, $NbSe_2$, and $NbTe_2$ are stable in the T structure. In fact, the prediction indicates that some of them do not exist in the commonly reported H structure but only in the T structure.

To the best of our knowledge, we report the first DFT structural and electronic study of 1D-MX_2 ribbons with stable T structure. Here we focus on a representative MX_2 compound, the $NiSe_2$. Theoretically, 2D-$NiSe_2$ can occur in both the T and H structure, with the T structure being ∼0.5 eV energetically more favorable.[3] Whereas $NiSe_2$ is a nonmagnetic metal in the H structure, the same compound is a narrow indirect band gap semiconductor in the T structure,[3] making it more attractive to possible electronic applications.

In this work, we are interested in 2D-MX_2 nanoribbons for several reasons. The first is to study the possibility of tailoring the electronic properties either by manipulating the width or by H saturation. The second is to look for a catalytic behavior due to the possibility of having metallic/chalcogenide edges in addition to the possibility of having magnetic effects. Previous experience with other nanoribbons obtained from 2D materials has shown that interesting effects arise,[38,39] so our study is also motivated by a natural curiosity about such interesting compounds, especially for centered honeycomb structures (T).

The outline of this manuscript is the following. We start with the reproduction of the centered honeycomb $NiSe_2$ single layer. We demonstrate the stability of ribbons of $NiSe_2$ with widths from 9 to 35 Å. Our ribbons present six different edge terminations for zigzaglike edges and two for armchair edges. The electronic properties of these eight families are presented. All these families were hydrogen-passivated. For the semiconductor ribbons we present the variation in band gap with the ribbon width. Electron densities and specific orbitals are also analyzed.

METHODOLOGY

In this work, all ab initio calculations were performed with the Quantum ESPRESSO[40] plane wave DFT and density functional perturbation theory (DFPT) code, available under the GNU Public License.[41] Scalar relativistic, spin polarized, and nonspin polarized calculations were performed for all the studied nanoribbons and 2D systems. The starting magnetization was randomly set to 1/2 on Ni type atoms. To include the spin−orbit interaction, the same calculations were performed using the full relativistic potentials. A plane-wave basis set with a cutoff of 612 eV was used. An ultrasoft pseudopotential[42] from the standard distribution generated using a modified RRKJ[43] approach and the generalized gradient approximation[44] (GGA) for the exchange-correlation functional in its PBE parametrization[45] were used. Calculations were done for 2D structures and both nanoribbons, bare and hydrogen-

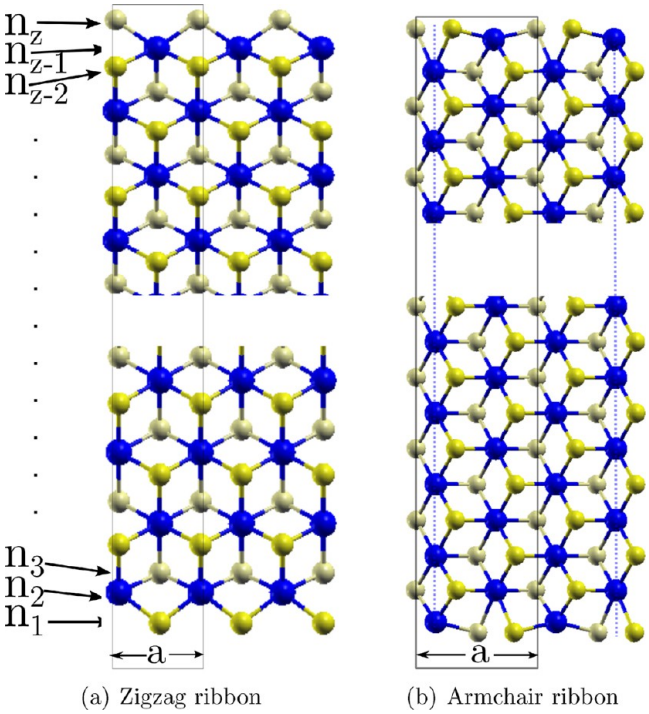

Figure 2. Nomenclature used to classify nanoribbons. Building blocks for the zigzag and armchair ribbons. For zigzag ribbons n_1, n_2, n_3, n_{z-2}, n_{z-1}, and n_z could be Se or Ni and z is the total number of rows in the nanoribbon. In the armchair case, the dotted line indicates if opposite edges present the Ni-aligned-Ni or Ni-centered-Se configurations. Large (blue) and small (yellow) circles represent Ni and Se atoms.

dx.doi.org/10.1021/jp409504f | J. Phys. Chem. C XXXX, XXX, XXX−XXX

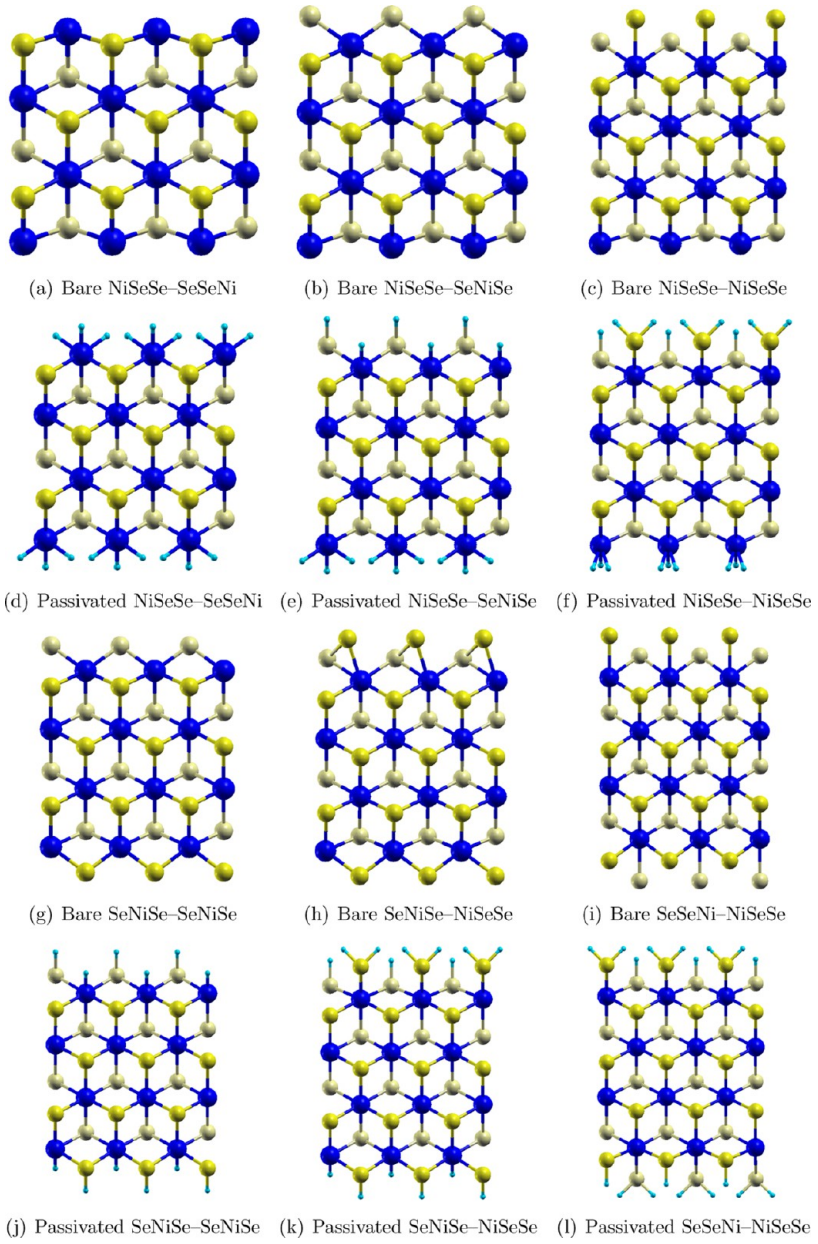

Figure 3. Graphical representation of the six root zigzag ribbons, both bare and H-passivated. Large (blue), medium (yellow), and small (aqua) circles represent Ni, Se, and H atoms, respectively.

passivated. All atomic positions and lattice parameters were optimized using the conjugate gradient method. The convergence for energy was chosen as 10^{-7} eV between two consecutive steps, and the maximum forces acting are smaller than 0.05 eV/Å. To test the reliability of this cutoff force, several structures were relaxed using forces smaller than 0.01 eV/Å; no fundamental differences with the 0.05 eV/Å cutoff were found. The stress in the periodic direction is in all cases lower than 0.01 GPa.

Rectangular supercells were built for the zigzag and armchair nanoribbons starting from the 2D T structure. The supercells were periodic in the x−direction, with lattice parameters a = 3.51 and a = 6.08 Å, respectively. To simulate isolated ribbons, the inplane and perpendicular distances between ribbons in adjacent supercells have to be larger than 10 Å. In the case of ribbons, the cell optimizations were just in the x-direction. The Brillouin zones of the unit cells were sampled by Monkhorst−Pack[46] grids of the form 16 × 16 × 1 for the 2D structures and 16 × 1 × 1 for the 1D structures. Depending on their width, ribbons present different edge terminations, defining the ribbon *families*. Six possible edge terminations are found for the zigzag ribbons and two for the armchair; therefore, here we studied six zigzag families and two armchair families. All ribbons were also hydrogen-passivated.

Figure 1 shows the structure in the xy and xz planes of the T and H configurations. We classified the zigzag terminations according to the three bottom atomic lines and the three top atomic lines (Figure 2a). The ribbon with bottom n_1−n_2−n_3 atoms lines (y-direction as reference) and top n_{z-2}−n_{z-1}−n_z atoms lines is called $n_1n_2n_3$−$n_{z-2}n_{z-1}n_z$ ribbon, where n_1, n_2, n_3, n_{z-2}, n_{z-1}, and n_z could be Se or Ni and z is the total number of rows in the nanoribbon. Zigzag ribbons have the restriction that $n_1n_2n_3$ and $n_{z-2}n_{z-1}n_z$ occurs in the cyclic order NiSeSe because

dx.doi.org/10.1021/jp409504f | J. Phys. Chem. C XXXX, XXX, XXX−XXX

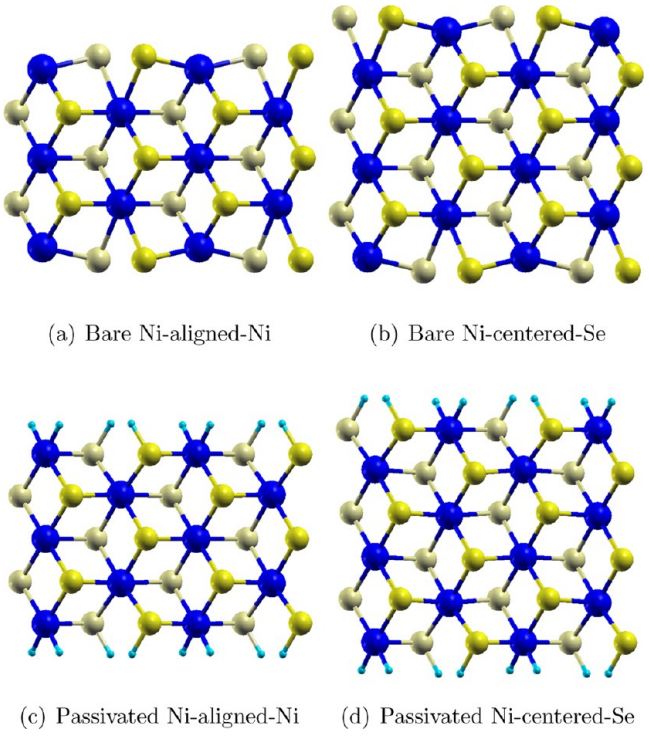

Figure 4. Graphical representation structure of the two root armchair ribbons, both bare and H-passivated. Large (blue), medium (yellow), and small (aqua) circles are Ni, Se, and H atoms, respectively.

of the crystal periodicity. The six representative zigzag edge terminations are shown in Figure 3.

In the case of armchair nanoribbons, two representative families appear; we call them Ni-aligned-Ni and Ni-centered-Se (Figure 2b). We chose this nomenclature according to the atomic symmetry of the opposite edges with the dotted lines in Figure 2.

Eight *root* ribbons were built as case studies to characterize the edge structure and electronic properties of each family; six for the zigzag families and two for the armchair families (Figures 3 and 4, respectively). Throughout this work we will mainly work with these eight ribbons. After structure relaxation of the root ribbons, their electronic properties were investigated. All root nanoribbons were hydrogen passivated to satisfy the surface dangling bonds. The hydrogen-passivated ribbons were also relaxed, and their electronic properties were investigated. The semiconductor ribbons are expanded to ~35 Å to find the variation of electronic band gap with ribbon width.

RESULTS AND DISCUSSION

Structure and Stability. To reproduce the results reported in ref 3, 2D-$NiSe_2$ sheets were built and geometry optimized in the T and H configurations (see Figure 1) with a total energy for the T structure 0.45 eV lower than that of the metastable H structure. In the T structure, the Ni−Se and Se−Se interatomic distances were 2.39 and 3.25 Å respectively, with a band gap of 0.11 eV. Metastable H-$NiSe_2$ presents Ni−Se and Se−Se interatomic distances of 2.41 and 2.63 Å, respectively, with a metallic behavior. Phonon modes for both structures were calculated to guarantee the stability. Negative frequencies were not found in either case, an indication of the stability of both structures. Without the spin−orbit interaction, all these results are in good agreement with those reported in ref 3, validating our calculations and the starting system for building our nanoribbons. The spin−orbit interaction was not considered in the report by Ataca et al.;[3] therefore, one cannot make comparisons in such cases. However, it is known that spin−orbit interaction is very important for transition-metal chalcogenide compounds in the band structure by splitting of the valence band.[47,48]

The cohesive energy of T and H systems relative to free constituent atoms was calculated as $E_C[NiSe_2] = E_T[Ni] + 2E_T[Se] - E_T[NiSe_2]$,[3] in terms of the total energy of $NiSe_2$, $E_T[NiSe_2]$, and total energies of free Ni and Se atoms, $E_T[Ni]$ and $E_T[Se]$, respectively. The cohesive energies are 12.51 and 12.06 eV for T and H structures, respectively, indicating a strong cohesion relative to free atoms of the constituents. A high cohesion energy is required for stability of the compound, but more important for the synthesis is the formation energy (E_f) with respect to bulk systems, calculated with the expression $E_f = E_C[NiSe_2] - E_C[Ni] - 2E_C[Se]$.[3] Natural references for the formation energy of this compound are the corresponding Ni and Se. The formation energy for T- and H-$NiSe_2$ systems are 0.81 and 0.36 eV, respectively; the higher the value, the more stable the system. Formation energies were also

Table 1. Cohesive and Formation Energies for 2D Systems, Bare and H-Passivated Zigzag and Armchair Nanoribbons, with the Corresponding Electronic Gap[a]

		cohesive energy per atom (eV)		formation energy per atom (meV)		electronic gap (eV)	
family	system name	bare	passivated	bare	passivated	bare	passivated
2D	T-$NiSe_2$	4.17	–	270.0	–	0.11	–
	H-$NiSe_2$	4.02	–	120.0	–	metal	–
zigzag	NiSeSe−seSeni	4.07	5.90	24.5	−93.7	metal	metal
	NiSeSe−SeNiSe	4.06	5.48	94.2	37.0	metal	metal
	NiSeSe−NiSeSe	3.97	5.59	78.1	67.1	metal	metal
	SeNiSe−SeNiSe	4.05	5.13	152.0	147.8	metal	0.25
	SeNiSe−NiSeSe	4.00	5.21	154.1	121.3	metal	0.30
	SeSeNi−NiSeSe	3.92	5.28	119.4	101.3	metal	metal
armchair	Ni-aligned-Ni	4.01	5.69	107.2	60.6	0.045	0.59
	Ni-centered-Se	4.04	5.44	135.4	101.2	0.061	0.38

[a]All these results are without spin−orbit interaction. The contribution of this interaction is about 0.011 eV in the total energy, and 2D-T-$NiSe_2$ becomes a metal. Band gaps in ribbons are also reduced on the order of 0.1 eV.

dx.doi.org/10.1021/jp409504f | J. Phys. Chem. C XXXX, XXX, XXX−XXX

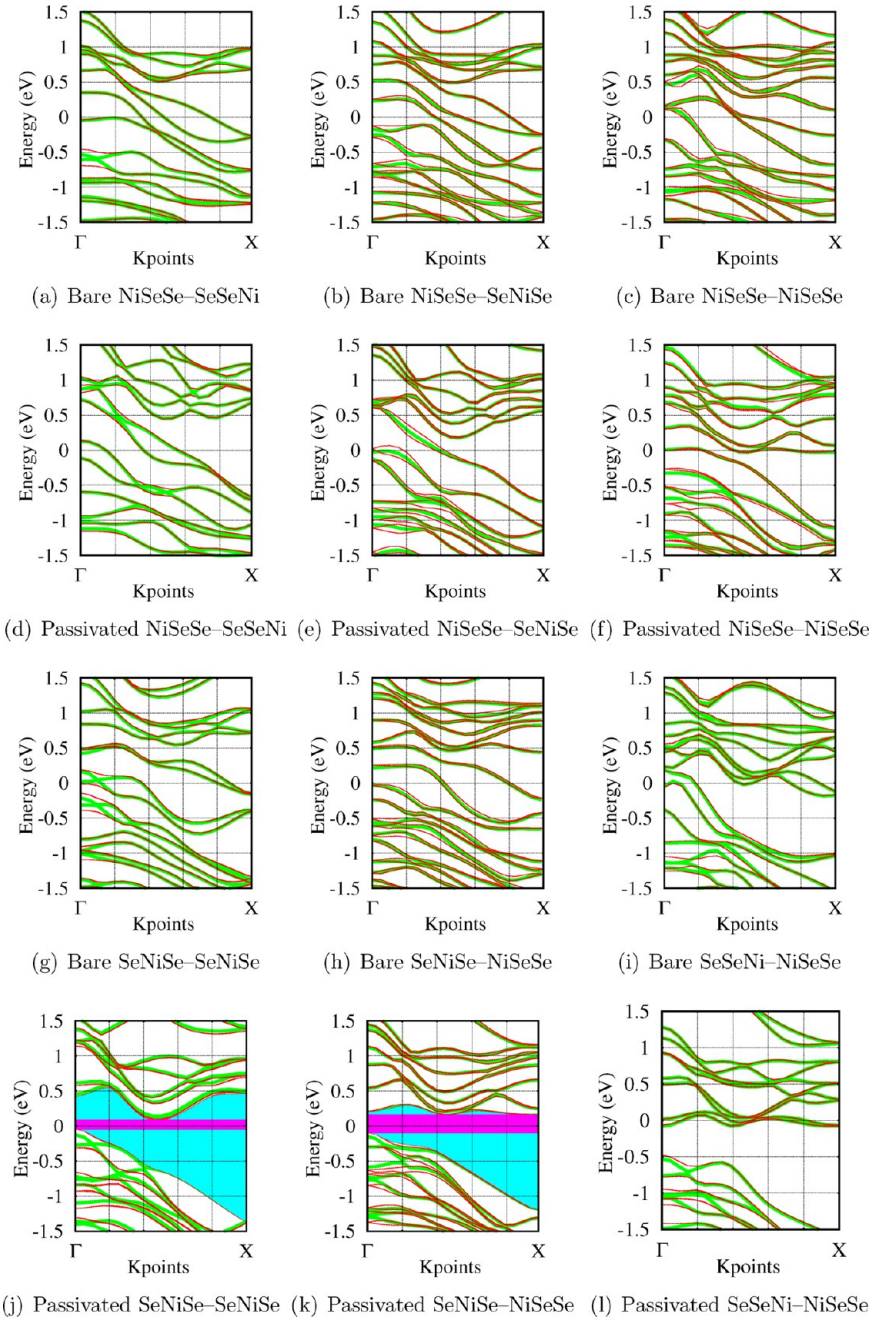

Figure 5. Electronic band structure for the corresponding six root zigzag ribbons, both bare and H-passivated. The red and green lines correspond to calculations with and without spin−orbit interaction, respectively. In the case of semiconductors (panels j and k), the energy gaps are highlighted (see Table 1).

calculated with the experimental values of cohesive energies from ref 49 as 3.20 and 2.74 eV for T and H structures, respectively. Both E_f values are positive, implying that T-$NiSe_2$ and H-$NiSe_2$ are stable and metastable, respectively, as previously reported by Ataca et al.[3]

We built our root nanoribbons by cutting them off the 2D sheet of the relaxed T-2D-$NiSe_2$ structure in the zigzag and armchair directions (Figures 3 and 4). Their E_C and E_f energies were calculated using the expressions $E_C = (nE_T[Ni] + mE_T[Se] + pE_T[H] - E_T[NiSe_2])/(n + m)$ and $E_f = (E_C[NiSe_2] - nE_C[Ni] - mE_C[Se] - pE_C[H])/(n + m)$, where n, m, and p are the number of Ni, Se, and H atoms, respectively; $p > 0$ only for H-passivated ribbons. For the E_f of hydrogen-terminated ribbons, we used our calculated binding energy for H_2 of 3.25 eV/atom. Bare ribbons present positive E_C ranging from 3.92 to 4.07 eV/atom, which indicates strong cohesion relative to the free constituents atoms (Table 1). The three bare root systems with lower cohesive energies are NiSeSe−NiSeSe, SeNiSe−NiSeSe, and SeNiSe−NiSeSe, all of which are characterized by two consecutive lines of semiconductor atoms at one or both of the edges. Table 1 also includes the E_f/atom for all bare ribbons. Bare SeNiSe−SeNiSe, SeNiSe−NiSeSe, and Ni-centered-Se nanoribbons present an E_f with values between the range of the T- and H-2D structures.

Relaxation of the armchair ribbon edges results in an increment of the edge Ni−Se distance of 1.67% with respect to

dx.doi.org/10.1021/jp409504f | J. Phys. Chem. C XXXX, XXX, XXX−XXX

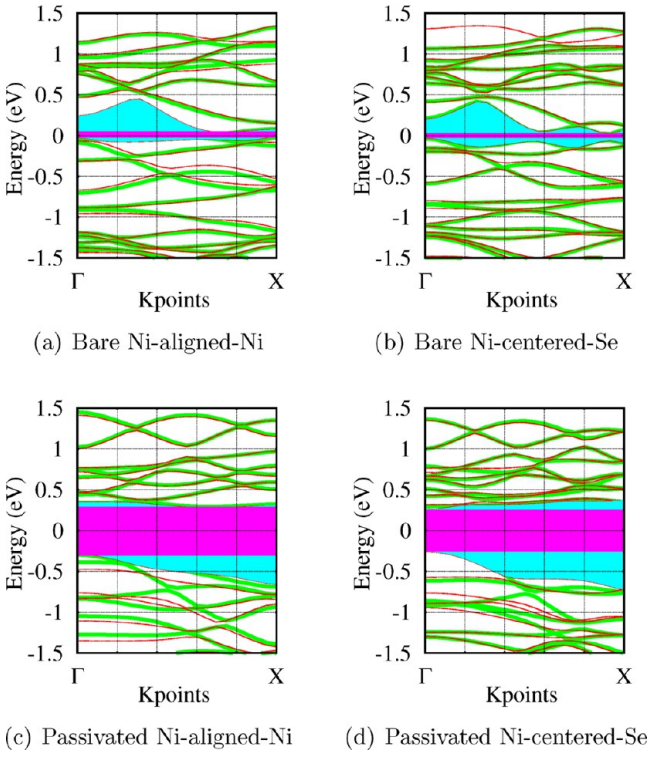

Figure 6. Electronic band structure for the corresponding two root armchair ribbons, both bare and H-passivated. The red and green lines correspond to calculations with and without spin−orbit interaction, respectively. The energy gaps are highlighted (see Table 1).

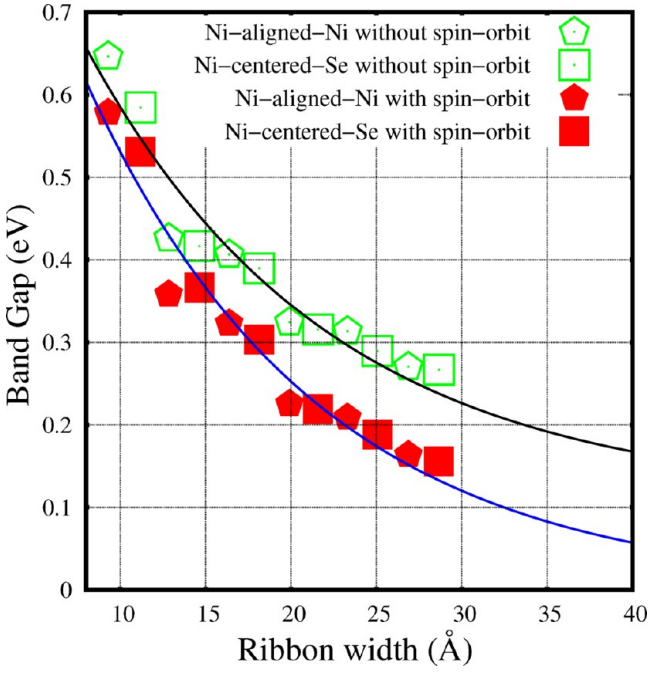

Figure 7. Band gaps of hydrogen passivated armchair ribbons as a function of width. The calculation without (green) and with (red) spin−orbit are included. The black (without) and blue (with spin−orbit interaction) solid lines are the corresponding fittings and are described within the text.

that of the bulk Ni−Se distance, while the edge Se−Ni−Se angle is reduced by 24%. As mentioned before, all root ribbons were hydrogen passivated. In the T-$NiSe_2$ 2D structure, each Ni

Table 2. Average Binding Energy for Different H-Passivation Densities for the Six Zigzag Nanoribbons[a]

	average binding energy of hydrogen (eV)			
	natural passivation	alternative passivation		
NiSeSe−SeSeNi	**H6 3.05**	H4 3.09	H2 3.06	
NiSeSe−SeNiSe	**H5 3.12**	H4 3.15	H3 3.18	
NiSeSe−NiSeSe	**H6 3.23**	H5 3.34	H4 3.38	H3 3.30
SeNiSe−SeNiSe	**H4 3.24**	H2-Ni 2.78	H2-Se 3.47	
SeNiSe−NiSeSe	**H5 3.16**	H4 3.26		
SeSeNi−NiSeSe	**H6 3.21**	H4 3.42		

[a]Natural passivations are indicated in bold.

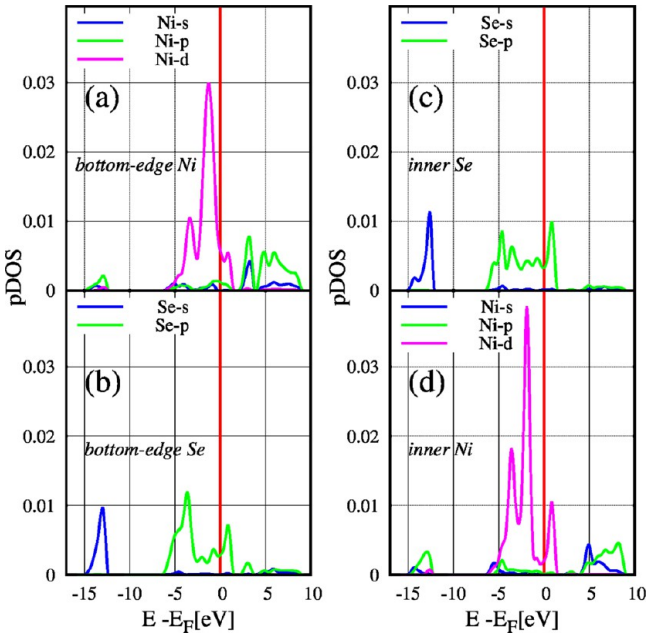

Figure 8. Partial density of states of NiSeSe−SeSeNi at edges and deep inside the nanoribbons for Ni and Se.

atom is bonded to six Se atoms and each Se atom is bonded to three Ni atoms. In contrast, ribbon edges present dangling bonds that were satisfied with hydrogens for passivation. We call *natural* passivation the one shown in Figure 3d−f,j−l and Figure 4c,d for zigzag and armchair ribbons, with a hydrogen atom added to the system to complete the six and three bonds for each Ni or Se edge atoms.

After H passivation and geometry relaxation of the ribbons, H−Se and H−Ni distances are ∼1.49 and ∼1.47 Å, respectively. According to Table 1, zigzag families with the terminations seen in Figure 3g,h are the only ones with a formation energy between the H and T structures. As a result, they are the most likely to be observed experimentally, as is confirmed by the fact that passivation easily sweeps edge states, leading to semiconductor nanoribbons. Such results are explained in a simple way by looking at the number of dangling bonds per unit length.[50−52] To do this, it is important to keep in mind that each Ni is coordinated with six Se by p−d hybridized ionic bonds. Thus, for cases a, b, c, and i in Figure 3, in at least one of the edges, three bonds are broken per unitary cell edge, whereas in cases g and h in Figure 3, two are produced. Thus, structures with outer Ni are discouraged because many bonds are cut for each Ni. Furthermore, such cuts produce a strong charge concentration at the Ni edge sites.

dx.doi.org/10.1021/jp409504f | J. Phys. Chem. C XXXX, XXX, XXX−XXX

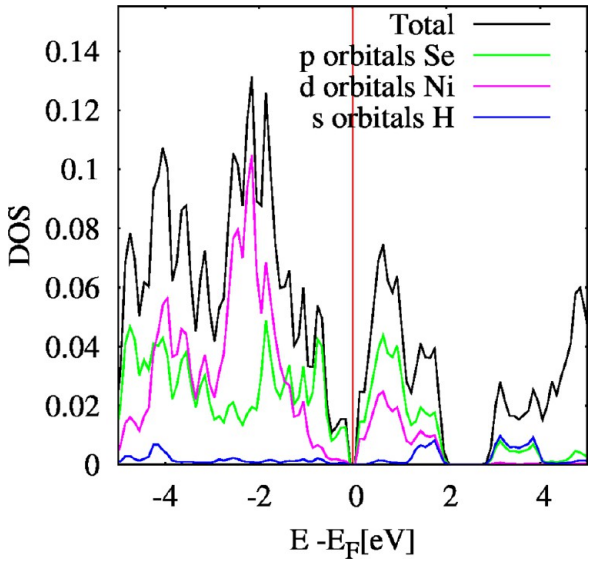

Figure 9. Total and partial density of states for the passivated zigzag SeNiSe−SeNiSe ribbon. The lowest valence band and the upper conduction bands are mainly Ni d-orbitals (magenta solid line) and Se p-orbitals (green solid line). Also, the H s-orbitals are presented (blue solid line).

All these facts are reflected in the crossing of bands at the Fermi energy (E_F), as will be explained in the following section.

Also, there is a clear effect in the edge structure because of edge interaction after geometry relaxation. In Figure 3h, two outer edge Se atoms connected to a Ni atom relax to form a typical homopolar Se−Se bond. However, while both edges in Figure 3i present termination the same as the reconstructed edge in Figure 3h, neither of its edges present reconstruction. This means that asymmetry of the edges around the center line is an important factor in stability. We have performed a scaling analysis, confirming that the imbalance is reduced as the width increases. Furthermore, for wide enough passivated ribbons with −NiSeSe edges, the outer Se atom dissociates from the edge in the form of SeH_2.

Electronic Properties. In this subsection we will discuss the resulting electronic properties for all possible nanoribbons structures, considering zigzag and armchair families. Before doing that, let us make an important remark concerning the possibility of magnetism in these structures. Band structures for all root systems were obtained using a random initial magnetization. The same results were found for spin-polarized and non-spin-polarized calculations. Thus, all considered systems are nonmagnetic, i.e., there is perfect spin degeneration. Also, calculations were made with and without spin−orbit interaction because there are reports of significant effects on similar compounds.[47,48]

The electronic band structures are shown in Figures 5 and 6 for zigzag and armchair ribbons, respectively. In the following subsections, we discuss these band structures.

Zigzag Nanoribbons. We can summarize our findings by pointing out that all root zigzag bare-terminated nanoribbons are metallic, as seen in Figure 5a−c,g−i. After *natural* hydrogen passivation, only two of them have an energy band gap: the SeNiSe−SeNiSe and SeNiSe−NiSeSe cases, corresponding to Figure 5j,k. The inclusion of the spin−orbit interaction preserves in a qualitative manner the electronic behavior, basically reducing the band gaps widths by at most 0.1 eV, which is a small change in contrast with other systems presenting corrections on the order of 0.5 eV.[47,48] In particular, zigzag nanoribbons are divided into two groups according to their edge topology: (i) those with outermost Ni atomic line (NiSeSe−SeSeNi, NiSeSe−SeNiSe, and NiSeSe−NiSeSe, Figure 3a−c, and their corresponding H passivations, Figure 3d−f) and (ii) those with outermost Se atomic lines (SeNiSe−SeNiSe, SeNiSe−NiSeSe, and SeSeNi−NiSeSe, Figure 3 g−i, and their corresponding passivations, Figure 3 j−l).

All bare and hydrogen passivated zigzag nanoribbons of the first group were found to be metallic, as seen in Figure 5 a−c,g−i, while within the group with outermost Se, H passivation causes metal−semiconductor transitions in two nanoribbons as shown in Figure 5j,k. These results and the corresponding gaps for the root systems are summarized in Table 1. According to those results, the stablest zigzag ribbon is the SeNiSe−SeNiSe, which is found to have semiconductor behavior for all calculated widths (Figure 7). In contrast, we found that as the width of the SeNiSe−NiSeSe ribbon increases, the system presents a semiconductor−metal transition at ∼23.55 Å.

These results point out the importance of the nanoribbon termination nature. For example, it is widely believed that semiconductor nanostructures always have a larger band gap than their bulk 2D values because of quantum confinement effects.[53] However, our results (without spin−orbit interaction) and a previous report indicate that bulk T-$NiSe_2$ is a semiconductor, while their corresponding nanoribbons are metallic. This is surprising because one would expect to recover the bulk behavior in the limit of an infinite width. This apparent paradox is explained in two ways. When the spin−orbit interaction is included, T-$NiSe_2$ turns out to be metallic; thus, the limit is obtained in a neat way. Without spin−orbit interaction, as reported by Ataca et al.,[3] such discrepancy can be easily explained by studying the nature of the states at the Fermi energy. As will be discussed below, such states are localized at the edges, as already suggested by the dispersive shape of highest valence and lowest conduction bands. Thus, as the width increases, the DOS at the Fermi energy goes to zero. Supporting our observation, we can cite that a similar situation occurs for MoS_2. From experiments and simulations, it is known that bulk 2D MoS_2 is a semiconductor whereas bare and hydrogenated zigzag nanoribbons are always metallic.[29,23] $NiSe_2$ is more complex than MoS_2 because in $NiSe_2$ T-like structures, the geometry allows edge atoms composed of chalcogenides, i.e., an outermost Se atomic line. In cases such as these, we have found that under passivation become semiconductors.

Before finishing this section, let us explore other possible edge hydrogen passivation densities for all root zigzag ribbons. The hydrogen binding energy (E_B) was used as an indicator of higher or lower stability, see Table 2, where the notation goes as follows: The *natural* hydrogenation for the ribbon is obtained by passivating Ni and Se outermost atoms, satisfying all dangling bonds, as indicated in Figure 3. The corresponding natural passivations are indicated in bold in Table 2. In such cases, the label H*N*, where N = 4, 5, or 6, denotes the number of hydrogens in the unitary cell. Alternative passivations are obtained by removing hydrogen atoms from natural edge passivations with more than one hydrogen. In such cases, the same notation H*N* is used to denote the total number of hydrogens, provided that the removal of bonds is symmetric in both edges. Table 2 also includes the special case SeNiSe−SeNiSe in which either Ni or Se is unpassivated, denoted by H2-Ni and H2-Se respectively. This was done to understand

dx.doi.org/10.1021/jp409504f | J. Phys. Chem. C XXXX, XXX, XXX−XXX

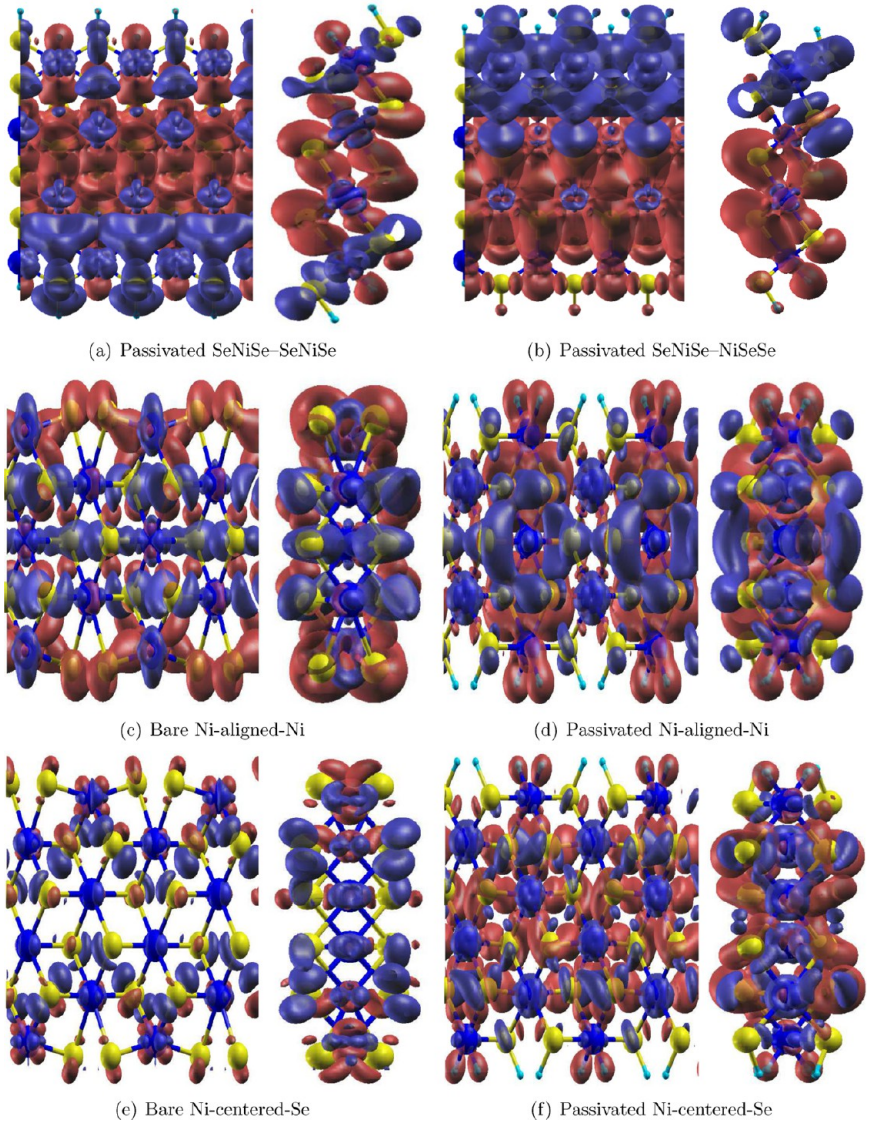

Figure 10. Charge density for the corresponding root zigzag and armchair semiconductors ribbons. Red and blue electronic clouds are maximum valence and minimum conduction bands, respectively. The isovalue for the surface is taken as 0.01 electron/Å^3. Large (blue), medium (yellow), and small (aqua) circles are Ni, Se, and H atoms, respectively.

why SeSeNi−NiSeSe nanoribbons returned to SeNiSe−SeNiSe by dissociation of SeH_2 molecules, as explained below.

From Table 2, we can summarize the results as follows: in general, the binding energy increases as the density decreases, except for H2 SeNiSe−SeNiSe. It is worth mentioning that all metallic passivated systems remained metallic and the two semiconductors became metallic when reducing the hydrogenation densities.

Armchair Nanoribbons. All calculated root armchair bare-termination nanoribbons, without considering spin−orbit interaction, are semiconductors with a very small band gap: 0.045 and 0.061 eV for Ni-aligned-Ni and Ni-centered-Se, respectively. The spin−orbit interaction reduces the band gaps and leads to metallic nanoribbons as expected for the bulk. Bare terminated armchair ribbons were built with widths from 10 to 30 Å, and only the root ribbons are semiconductors. In this work, the largest electronic band gap is for hydrogen-passivated armchair nanoribbons with gaps of 0.59 and 0.38 eV for passivated root Ni-aligned-Ni and passivated root Ni-centered-Se nanoribbons, respectively. In Figure 7, the variation of electronic band gap for hydrogen-passivated ribbons is reported. The tendency of the band gap without spin−orbit interaction for the armchair follows the expression $E(w) = 0.11 + ae^{-w/\lambda}$, where a = 0.96 eV, λ = 14.21 Å, and w is the ribbon width. Taking into account the spin−orbit interaction, the tendency is $E(w) = de^{-w/\lambda_{ls}}$, where d = 1.12 eV, λ_{ls} = 13.45 Å, and w is the ribbon width.

Overall Picture of Electronic Properties. All the electronic properties can be explained using some simple physical observations. There are three mechanisms that modulate the electronic properties of the nanoribbons when compared with those of the bulk material: (i) quantum confinement, (ii) edge topology, and (iii) interaction between edges. Quantum confinement is evident only for semiconducting nanoribbons, as was discussed previously, where the gap diminishes as the width increases. Without considering spin−orbit interaction, edge effects lead to metallic nanoribbons in an otherwise semiconducting material. This can be explained only if edge states appear inside the gap observed in the bulk but modulated by quantum confinement. Such gap filling can be understood in

dx.doi.org/10.1021/jp409504f | J. Phys. Chem. C XXXX, XXX, XXX−XXX

a rough way using the Lifshitz equation,[54] considering that edge atoms are similar to impurities. In the present case, edge states appear because of dangling bonds. As explained in the section on stability, lines of outer Ni atoms increase the number of broken p−d hybrid bonds per unit length, as in Figure 5a−c. In Figure 5g−i, edge states are still observed, but the bands are pushed to lower energies, as expected. To confirm the nature of states around E_F, we have computed the partial density of states (pDOS) at Ni and Se atoms at edges and deep inside the nanoribbons (Figure 8). The results in Figure 8d confirm the appearance of a pseudogap at E_F for Ni atoms inside the nanoribbon, whereas the pseudogap is filled for Ni at the edges (see Figure 8a). As can be seen in Figure 8a,b, edge states are made mainly from d states of the Ni with a contribution from p states of Se, as expected. For semiconducting ribbons, the states near the bandgap are also dominated by Ni d orbitals and Se p orbitals, as seen in Figure 9.

An analysis of the charge for states near E_F indicates how the interaction between edges can be very important for narrow systems. For example, in Figures 5j,k and 6a−d, we show the band structure of the semiconductor root systems with the highest occupied and the lowest unoccupied bands. The highest occupied and lowest unoccupied orbitals are also illustrated in Figure 10. The SeNiSe−SeNiSe root ribbon presents a symmetrical distribution of both orbitals with respect to the x axis. In contrast, the SeNiSe−NiSeSe system shows an accumulation of the top valence orbital on the ribbon's bottom SeNiSe edge, whereas the bottom conduction orbital localizes on the ribbon's top NiSeSe edge. Both systems are indirect semiconductors.

Regarding the armchair ribbons, the band structure and highest occupied and lowest unoccupied orbitals are also shown in Figure 6. In this case, all the ribbons present symmetry of the orbitals with respect to the x axis and the band gaps are indirect.

Concerning the possibility of applications, some recent studies[6,7] show that centered honeycomb nanostructures enhance electrocatalytic activity because of the high concentration of metallic edges. This suggests that in the present study, NiSeSe−SeSeNi will be the best candidate as a catalyst for hydrogen evolution, but NiSeSe−SeNiSe and NiSeSe−NiSeSe will also be used for the same process.

SUMMARY

This work pioneers the ab initio studies of centered honeycomb nanoribbons, defining the representative ribbon's families and opening the field to study to other systems in the T structure. In this work, we use first-principles calculations with and without spin−orbit interaction to explore the different atomic arrangements for $NiSe_2$ nanoribbons in the stable T crystalline structure. Zigzag bare-nanoribbons geometrical reconstruction leads to metallic systems, whereas just two hydrogen-passivated nanoribbons are semiconductors. NiSeSe−SeSeNi has the largest metallic edge, suggesting that this ribbon could be a possible candidate as a catalyst for hydrogen evolution. SeNiSe−SeNiSe is the stablest zigzag nanoribbon. Studies of edge H passivation densities reveals that SeSeNi− edges are prone to convert to SeNiSe by a SeH_2 desorption mechanism. Only thin bare armchair nanoribbons are semiconductors with a very small band gap (0.045 and 0.061 eV); thicker nanoribbons are metals. When armchair ribbons are hydrogen-passivated, the band gaps increase considerably to values up to ∼0.6 eV. The study of the variation in electronic band gap with the width was done, and we report the asymptotic tendency to T-$NiSe_2$ band gap (0.11 eV) for armchair passivated nanoribbons. All these results are explained in terms of three basic mechanisms: quantum confinement, edge topology, and, for narrow nanoribbons, by the interaction between edges because of an asymmetrical distribution of charges. Also, we found that the inclusion of the spin−orbit interaction indicates that the bulk T-$NiSe_2$ is a metal instead of a semiconductor as was reported in a previous calculation that did not include such relativistic effects.[47] The identification of possible nanoribbons as a catalyst suggests that more work is needed to elucidate its properties, such as the identification of Raman-active modes. Such properties will be the subject of future research.

ASSOCIATED CONTENT

Supporting Information

Comparison of the band structure in T-$NiSe_2$ with and without spin−orbit interaction (Figure S1). This material is available free of charge via the Internet at http://pubs.acs.org.

AUTHOR INFORMATION

Corresponding Author

*E-mail: angelreyes@fisica.unam.mx.

Notes

The authors declare no competing financial interest.

ACKNOWLEDGMENTS

The authors thank DGTIC-UNAM. J.A.R.-R. acknowledges support from DGAPA-UNAM. G.G.N. acknowledges support from DGAPA-UNAM Project 102513. This work was completed under the support of FICSAC with the program *Attraction of Visiting Academics 2012* and by the Physics and Mathematics Department of UIA.

REFERENCES

(1) Wilson, J.; AD, Y. The Transition Metal Dichalcogenides Discussion and Interpretation of the Observed Optical, Electrical and Structural Properties. *Adv. Phys.* **1969**, *18*, 193−335.
(2) Mattheiss, L. F. Band Structures of Transition-Metal-Dichalcogenide Layer Compounds. *Phys. Rev. B* **1973**, *8*, 3719−3740.
(3) Ataca, C.; Sahin, H.; Ciraci, S. Stable, Single-Layer MX_2 Transition-Metal Oxides and Dichalcogenides in a Honeycomb-Like Structure. *J. Phys. Chem. C* **2012**, *116*, 8983−8999.
(4) Lebègue, S.; Eriksson, O. Electronic Structure of Two-dimensional Crystals from *ab initio* Theory. *Phys. Rev. B* **2009**, *79*, 115409.
(5) Novoselov, K. S.; Jiang, D.; Schedin, F.; Booth, T. J.; Khotkevich, V. V.; Morozov, S. V.; Geim, A. K. Two-Dimensional Atomic Crystals. *Proc. Natl. Acad. Sci. U.S.A.* **2005**, *102*, 10451−10453.
(6) Lukowski, M.; Daniel, A.; Meng, F.; Forticaux, A.; Li, L.; Jin, S. Enhanced Hydrogen Evolution Catalysis from Chemically Exfoliated Metallic MoS_2 Nanosheets. *J. Am. Chem. Soc.* **2013**, *135*, 10274−10277.
(7) Voiry, D.; Yamaguchi, H.; Li, J.; Silva, R.; Alves, D.; Fujita, T.; Chen, M.; Asefa, T.; Shenoy, V.; Eda, G.; et al. Enhanced Catalytic Activity in Strained Chemically Exfoliated WS_2 Nanosheets for Hydrogen Evolution. *Nat. Mater.* **2013**, *12*, 850−855.
(8) Novoselov, K. S.; Geim, A. K.; Morozov, S. V.; Jiang, D.; Zhang, Y.; Dubonos, S. V.; Grigorieva, I. V.; Firsov, A. A. Electric Field Effect in Atomically Thin Carbon Films. *Science* **2004**, *306*, 666−669.
(9) Osada, M.; Sasaki, T. Exfoliated Oxide Nanosheets: New Solution to Nanoelectronics. *J. Mater. Chem.* **2009**, *19*, 2503−2511.
(10) Li, X.; Cai, W.; An, J.; Kim, S.; Nah, J.; Yang, D.; Piner, R.; Velamakanni, A.; Jung, I.; Tutuc.; et al. Large-Area Synthesis of High-

Quality and Uniform Graphene Films on Copper Foils. *Science* **2009**, *324*, 1312−1314.
(11) Lee, Y.-H.; Zhang, X.-Q.; Zhang, W.; Chang, M.-T.; Lin, C.-T.; Chang, K.-D.; Yu, Y.-C.; Wang, J. T.-W.; Chang, C.-S.; Li.; et al. Lain-Jong Synthesis of Large-Area MoS_2 Atomic Layers with Chemical Vapor Deposition. *Adv. Mater.* **2012**, *24*, 2320−2325.
(12) Coleman, J. N.; Lotya, M.; ONeill, A.; Bergin, S. D.; King, P. J.; Khan, U.; Young, K.; Gaucher, A.; De, S.; Smith, R. J.; et al. Two-Dimensional Nanosheets Produced by Liquid Exfoliation of Layered Materials. *Science* **2011**, *331*, 568−571.
(13) Nicolosi, V.; Chhowalla, M.; Kanatzidis, M. G.; Strano, M. S.; Coleman, J. N. Liquid Exfoliation of Layered Materials. *Science* **2013**, *340*, 1226419.
(14) Britnell, L.; Gorbachev, R.; Jalil, R.; Belle, B.; Schedin, F.; Mishchenko, A.; Georgiou, T.; Katsnelson, M.; Eaves, L.; Morozov, S.; et al. Field-Effect Tunneling Transistor Based on Vertical Graphene Heterostructures. *Science* **2012**, *335*, 947−950.
(15) Vogt, P.; De Padova, P.; Quaresima, C.; Avila, J.; Frantzeskakis, E.; Asensio, M. C.; Resta, A.; Ealet, B.; Le Lay, G. Silicene: Compelling Experimental Evidence for Graphenelike Two-Dimensional Silicon. *Phys. Rev. Lett.* **2012**, *108*, 155501.
(16) Dean, C. R.; Young, A. F.; Meric, I.; Lee, C.; Wang, L.; Sorgenfrei, S.; Watanabe, K.; Taniguchi, T.; Kim, P.; Shepard, K. L; Boron, J. H. Nitride Substrates for High-quality Graphene Electronics. *Nat. Nanotechnol.* **2010**, *5*, 722−726.
(17) Naumis, G. G. Internal Mobility Edge in Doped Graphene: Frustration in a Renormalized Lattice. *Phys. Rev. B* **2007**, *76*, 153403.
(18) Barrios-Vargas, J. E.; Naumis, G. G. Doped graphene: The Interplay Between Localization and Frustration Due to the Underlying Triangular Symmetry. *J. Phys.: Condens. Matter* **2011**, *23*, 375501.
(19) Barrios-Vargas, J.; Naumis, G. G. Pseudo-gap Opening and Dirac Point Confined States in Doped Graphene. *Solid State Commun.* **2013**, *162*, 23−27.
(20) Bostwick, A.; McChesney, J. L.; Emtsev, K. V.; Seyller, T.; Horn, K.; Kevan, S. D.; Rotenberg, E. Quasiparticle Transformation During a Metal-Insulator Transition in Graphene. *Phys. Rev. Lett.* **2009**, *103*, 056404.
(21) López-Rodríguez, F.; Naumis, G. Graphene under perpendicular incidence of electromagnetic waves: Gaps and band structure. *Philos. Mag.* **2010**, *90*, 2977−2988.
(22) López-Rodríguez, F. J.; Naumis, G. G. Analytic Solution for Electrons and Holes in Graphene under Electromagnetic Waves: Gap Appearance and Nonlinear Effects. *Phys. Rev. B* **2008**, *78*, 201406.
(23) Mak, K. F.; Lee, C.; Hone, J.; Shan, J.; Heinz, T. F. Atomically Thin MoS_2: A New Direct-Gap Semiconductor. *Phys. Rev. Lett.* **2010**, *105*, 136805.
(24) Tongay, S.; Zhou, J.; Ataca, C.; Lo, K.; Matthews, T. S.; Li, J.; Grossman, J. C.; Wu, J. Thermally Driven Crossover from Indirect toward Direct Bandgap in 2D Semiconductors: $MoSe_2$ versus MoS_2. *Nano Lett.* **2012**, *12*, 5576−5580.
(25) Sundaram, R. S.; Engel, M.; Lombardo, A.; Krupke, R.; Ferrari, A. C.; Avouris, P.; Steiner, M. Electroluminescence in Single Layer MoS_2. *Nano Lett.* **2013**, *13*, 1416−1421.
(26) Han, M. Y.; Özyilmaz, B.; Zhang, Y.; Kim, P. Energy Band-Gap Engineering of Graphene Nanoribbons. *Phys. Rev. Lett.* **2007**, *98*, 206805.
(27) Son, Y.-W.; Cohen, M. L.; Louie, S. G. Energy Gaps in Graphene Nanoribbons. *Phys. Rev. Lett.* **2006**, *97*, 216803.
(28) Nakada, K.; Fujita, M.; Dresselhaus, G.; Dresselhaus, M. S. Edge State in Graphene Ribbons: Nanometer Size Effect and Edge Shape Dependence. *Phys. Rev. B* **1996**, *54*, 17954−17961.
(29) Botello-Méndez, A. R.; López-Urías, F.; Terrones, M.; Terrones, H. Metallic and Ferromagnetic Edges in Molybdenum Disulfide Nanoribbons. *Nanotechnology* **2009**, *20*, 325703.
(30) Yue, Q.; Chang, S.; Kang, J.; Zhang, X.; Shao, Z.; Qin, S.; Li, J. Bandgap Tuning in Armchair MoS_2 Nanoribbon. *J. Phys.: Condens. Matter* **2012**, *24*, 335501.
(31) Hromadová, L.; Martonak, R.; Tosatti, E. Structure change, layer sliding, and metallization in high-pressure MoS_2. *Phys. Rev. B* **2013**, *87*, 144105.
(32) Ataca, C.; Sahin, H.; Akturk, E.; Ciraci, S. Mechanical and Electronic Properties of MoS_2 Nanoribbons and Their Defects. *J. Phys. Chem. C* **2011**, *115*, 3934−3941.
(33) Koski, K. J.; Wessells, C. D.; Reed, B. W.; Cha, J. J.; Kong, D.; Cui, Y. Chemical Intercalation of Zerovalent Metals into 2D Layered Bi_2Se_3 Nanoribbons. *J. Am. Chem. Soc.* **2012**, *134*, 13773−13779.
(34) She, G.; Zhang, X.; Shi, W.; Cai, Y.; Wang, N.; Liu, P.; Chen, D. Template-Free Electrochemical Synthesis of Single-Crystal CuTe Nanoribbons. *Cryst. Growth Des.* **2008**, *8*, 1789−1791.
(35) Podberezskaya, N.; Magarill, S.; Pervukhina, N.; Borisov, S. Crystal Chemistry of Dichalcogenides MX_2. *J. Struct. Chem.* **2001**, *42*, 654−681.
(36) Ding, Y.; Wang, Y.; Ni, J.; Shi, L.; Shi, S.; Tang, W. First Principles Study of Structural, Vibrational and Electronic Properties of Graphene-like $\{MX_2\}$ (M=Mo, Nb, W, Ta; X=S, Se, Te) Monolayers. *Phys. B (Amsterdam, Neth.)* **2011**, *406*, 2254−2260.
(37) Yun, W. S.; Han, S. W.; Hong, S. C.; Kim, I. G.; Lee, J. D. Thickness and Strain Effects on Electronic Structures of Transition Metal Dichalcogenides: 2H-MX_2 Semiconductors (M = Mo, W; X = S, Se, Te). *Phys. Rev. B* **2012**, *85*, 033305.
(38) Naumis, G. G.; Terrones, M.; Terrones, H.; Gaggero-Sager, L. M. Design of Graphene Electronic Devices using Nanoribbons of Different Widths. *Appl. Phys. Lett.* **2009**, *95*, 182104−182104−3.
(39) Cresti, A.; Nemec, N.; Biel, B.; Niebler, G.; Triozon, F.; Cuniberti, G.; Roche, S. Charge Transport in Disordered Graphene-Based Low Dimensional Materials. *Nano Res.* **2008**, *1*, 361−394.
(40) Giannozzi, P.; Baroni, S.; Bonini, N.; Calandra, M.; Car, R.; Cavazzoni, C.; Ceresoli, D.; Chiarotti, G. L.; Cococcioni, M.; Dabo, I.; et al. QUANTUM ESPRESSO: A Modular and Open-source Software Project for Quantum Simulations of Materials. *J. Phys.: Condens. Matter* **2009**, *21*, 395502.
(41) Free Software Foundation. GNU General Public License. http://www.gnu.org/licenses/gpl.html.
(42) Vanderbilt, D. Soft Self-Consistent Pseudopotentials in a Generalized Eigenvalue Formalism. *Phys. Rev. B* **1990**, *41*, 7892−7895.
(43) Rappe, A. M.; Rabe, K. M.; Kaxiras, E.; Joannopoulos, J. D. Optimized Pseudopotentials. *Phys. Rev. B* **1990**, *41*, 1227−1230.
(44) Perdew, J. P.; Chevary, J. A.; Vosko, S. H.; Jackson, K. A.; Pederson, M. R.; Singh, D. J.; Fiolhais, C. Atoms, Molecules, Solids, and Surfaces: Applications of the Generalized Gradient Approximation for Exchange and Correlation. *Phys. Rev. B* **1992**, *46*, 6671−6687.
(45) Perdew, J. P.; Burke, K.; Ernzerhof, M. Generalized Gradient Approximation Made Simple. *Phys. Rev. Lett.* **1996**, *77*, 3865−3868.
(46) Monkhorst, H. J.; Pack, J. D. Special Points for Brillouin-Zone Integrations. *Phys. Rev. B* **1976**, *13*, 5188−5192.
(47) Zhu, Z. Y.; Cheng, Y. C.; Schwingenschlögl, U. Giant Spin-Orbit-Induced Spin Splitting in Two-Dimensional Transition-Metal Dichalcogenide Semiconductors. *Phys. Rev. B* **2011**, *84*, 153402.
(48) Radzyński, T.; Łusakowski, A. Influence of Spin-Orbit Interaction on Band Structure and Elastic Properties of PbTe. *Acta Phys. Pol., A* **2009**, *116*, 954−955.
(49) Kittel, C.; McEuen, P. *Introduction to Solid State Physics*, 8th ed.; Wiley: New York, 2005.
(50) Kerner, R.; Naumis, G. G. Stochastic Matrix Description of the Glass Transition. *J. Phys.: Condens. Matter* **2000**, *12*, 1641.
(51) Naumis, G. G.; Kerner, R. Stochastic Matrix Description of Glass Transition in Ternary Chalcogenide Systems. *J. Non-Cryst. Solids* **1998**, *231*, 111−119.
(52) Huerta, A.; Naumis, G. G. Evidence of a Glass Transition Induced by Rigidity Self-Organization in a Network-Forming Fluid. *Phys. Rev. B* **2002**, *66*, 184204.
(53) Deng, H.-X.; Li, S.-S.; Li, J.; Wei, S.-H. Effect of Hydrogen Passivation on the Electronic Structure of Ionic Semiconductor Nanostructures. *Phys. Rev. B* **2012**, *85*, 195328.
(54) Economou, E. N. *Green's Functions in Quantum Physics*; Springer: Berlin, 1984; Vol. 3.